ontario hydro
research division

COMPLIMENTARY COPY
Please Credit Ontario Hydro Research if
Reproduced in Whole or in Part

To: Mr. E.M. Kurak
Acting Manager - Transmission Lines
Transmission Operations Division

OVERHEAD CONDUCTOR AMPACITY STUDIES IV
Interpretation of 1986 Summer Data

W.A. Chisholm and J.S. Barrett

Electrical Research Department

The Bulk Electrical System contains many older circuits that have a maximum conductor temperature limit of 49°C. A program of measurements and modeling has been initiated to allow best use of these lines during summer peak-load conditions. Misapplication of the ruling-span approximation to lines with unequal span lengths leads to errors in sag changes with temperature. These errors could require derating of lines like the Essa Test Line from 49°C to 40°C. Predictions of conductor temperature based on Out-Of-Limits Monitoring (OOLM) weather data are usually higher than observed. However, OOLM predictions were too low by more than 4 C° on 37 of 864 test hours. Of the 37 periods, 13 were daylight hours with the worst cases having conductor temperatures of 39-41°C and an OOLM-based predictions of 30-36°C.

INTRODUCTION

Many older lines in the Bulk Electrical System were designed and constructed for low maximum operating temperatures. At that time, utilities thought that an undesirable annealing process would occur if conductor operating temperatures exceeded 49°C (120°F). The annealing temperature limit is now known to be higher. However, clearance requirements to ground still limit the safe and economical operation of these lines. The problems are particularly acute in summer conditions. High ambient temperatures combined with low wind speeds or high solar input lead to reduced clearances and restricted power flows at times of peak air-conditioning load.

job	file	date	report no.
17-164-231	812.2	December 1, 1987	87-230-K

In previous work, we initiated a program of continuous data measurement. A spare 115-kV single-circuit test line was energized at 240 V with a circulating current of 260 A. The program then developed instrumentation for the parameters that affect conductor temperature: ambient temperature, solar input, current, wind speed and direction. A clearance measurement was also performed continuously to relate conductor temperature to sag.

PREVIOUS WORK

Figure 1 shows a block diagram of the work performed to date. In 1985 /1/, instrumentation was applied to the line. Predictions of weather from the Out-of-Limits Monitoring (OOLM) weather monitoring system were also saved. Conductor cooling models /2,3/ were shown to be valid, provided that the actual conditions at the conductor were used as input. Site weather data and OOLM predictions agreed on average in both 1985 and 1986 /4/. The reduction factors applied to OOLM wind speeds cause over-estimation of conductor temperatures, although there were some periods where the conductor temperature estimate is too low. The most important discrepancy, however, concerns the relationship between clearance and temperature.

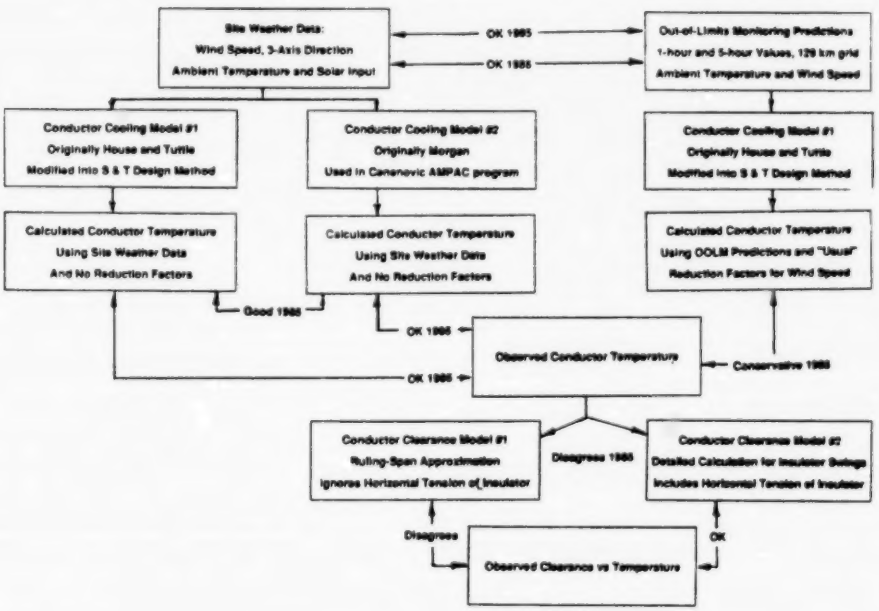

Figure 1: Ampacity Study Modules

When operating transmission lines, changes in clearance with temperature are now estimated using a sag-tension calculation based on the ruling-span approximation. In 115-kV lines with mixed long and short spans, the ruling-span approximation leads to significant errors. For example, on our test line, Table 1 shows that the ruling-span sag-temperature coefficients are 20% high on the longest span and 30% low on the shortest span.

Table 1

Comparison of Sag-Temperature Models for Essa Test Line
Ruling Span = 273 m.

Span Length (m)	Sag-Temperature Coefficient - mm/°C from 20° to 50°C	
	Ruling-Span Approximation	Accurate Calculation
164 m	10.6 mm/°C	15.2 mm/°C
361 m	51.8 mm/°C	43.1 mm/°C

The 5-9 mm/°C differences in the temperature coefficients lead to clearance uncertainties of 130-250 mm at 49°C. While these seem like small uncertainties, they represent operating temperature differences of -9 and +5°C. If a ruling-span analysis done at 20°C rated every span of our test line at 49°C, we could operate our longest span at 54°C but should derate the shortest span to 40°C based on the accurate calculation. The discrepancy in sag-temperature modelling is the most important finding of these studies.

Accurate calculation of sag-temperature relationships was outlined in Research Division Report 86-91-K /1/ and originally by Winkleman /5/. The ruling-span approximation states that the sag of any span can be estimated as proportional to the square of the ratio of span length to a "ruling-span" length A_r from Equation (1):

$$A_r = \frac{\sqrt{A_1^3 + A_2^3 + \cdots + A_n^3}}{\sqrt{A_1 + A_2 + \cdots + A_n}} \tag{1}$$

When temperatures increase from the stringing temperature, the conductor expands and its axial tension decreases. For lines with equal-length spans, the suspension insulators do not swing from vertical because horizontal tensions are balanced. When spans are not equal, insulators swing to equalize horizontal components. The ruling-span model assumes incorrectly that complete equalization is achieved, thus overstating the amount of insulator swing. There will be a difference in horizontal tension components of the two adjacent spans, equal to the small horizontal tension component along the insulator string as follows:

$$\delta H = W_c \tan(\theta) \tag{2}$$

In Equation 2, W_c is the weight of conductor between low points of the two adjacent spans and θ is the insulator swing from vertical. To quote Winkelman /5/,

> Where the spans in a series of suspension spans vary considerably in length, the tension in the extremely long and short spans will not be fully equalized to that of the ruling span and considerable error can result in design clearances. .... The extremely long spans will have greater cold-weather sag and smaller hot-weather sag than anticipated; the opposite will be true for the short spans.

Ruling-span inaccuracies are largest for lines with short insulator strings, since in effect the ruling-span approximation is assuming an infinite string length. Our 115-kV transmission lines are most affected by the errors. These lines tend to be the oldest in the Bulk Electrical System, and are most likely to have a present rating of 49°C.

The calculation of sag-tension relationships involves iterative solution of a nonlinear problem. Appendix 1 provides a general formulation of the accurate solution along with an iteration plan. Solutions for 40 spans can be obtained by using a personal computer for a few minutes.

VERIFICATION OF SAG-TEMPERATURE MODEL

The clearance measurements for the shortest test span were performed at midspan. The weight of the instrumentation mounted there affects the sag-temperature coefficient. A rough model for the effect is that the span is extended by the instrument weight divided by the conductor weight per unit length. With the 40.6 kg mass of the instrumentation and the 0.975 kg/m weight of 477-kcmil conductor, the additional length works out to 42 m. For calculating the sag-temperature behaviour with weight at midspan, the accurate model described in Reference 1 was used.

The ruling-span approximation predicts that the sag-temperature coefficient of the loaded test span will be 15.6 mm/°C. The accurate calculation predicts a value of 18.9 mm/°C. After matching both models to a clearance of 7.03 m at 20°C, we see in Figure 2 that the accurate model runs through the center of the data. Data points were selected on the basis of close agreement between average and minimum clearance during the 15-minute recording periods. This eliminated readings from periods when the sonar instrument was swinging in the wind. A linear regression of the 2150 data points gives a slope of -18.7 mm/°C with an intercept of 7.41 m. The standard deviation of the slope was 0.1 mm/°C and the intercept deviation was 2.7 mm.

Figure 2 also shows that the tested span has 6.5 m of clearance at 49°C. This provides a 1.0-m margin over the CSA Standard C22.3 limit of 5.5 m. Thus, our test line does not need to be derated. However, most lines with a 49°C rating will have several spans that have no existing margin left for meeting CSA clearance requirements. If any of these critical spans are shorter than the ruling span, then derating of operating temperatures is required. Conversely, if all critical spans are longer than the ruling span, increased operating temperatures could be used.

An analysis of sag-temperature coefficient changes from day to day is shown in Figure 3. Each day, a linear regression was calculated for valid clearance measurements. The resulting sag-temperature coefficients vary from 15.2 up to 20.9 mm/°C. The mean value is 18.3 mm/°C. We computed a standard deviation of 1.4 mm/°C, which is somewhat larger than the standard deviations of each day and much larger than the linear regression for the whole period. Figure 3 shows a plot of sag-temperature coefficient versus the average conductor temperature over the 24-hour regression period.

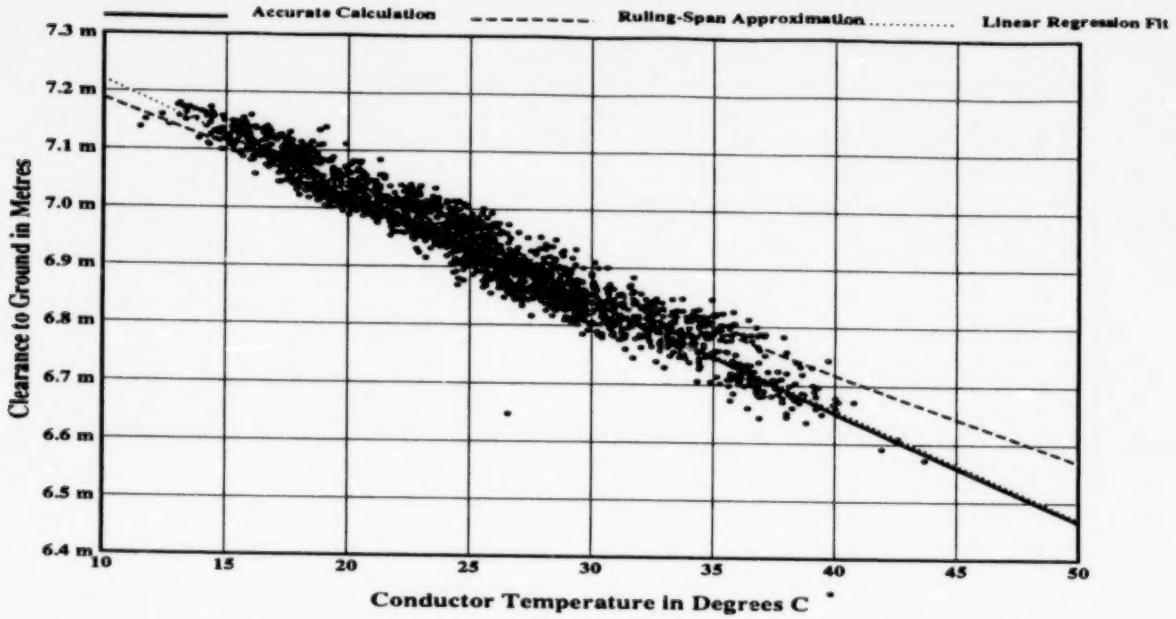

Figure 2: Clearance vs Conductor Temperature
164-m Test Span with 40-kg Instruments

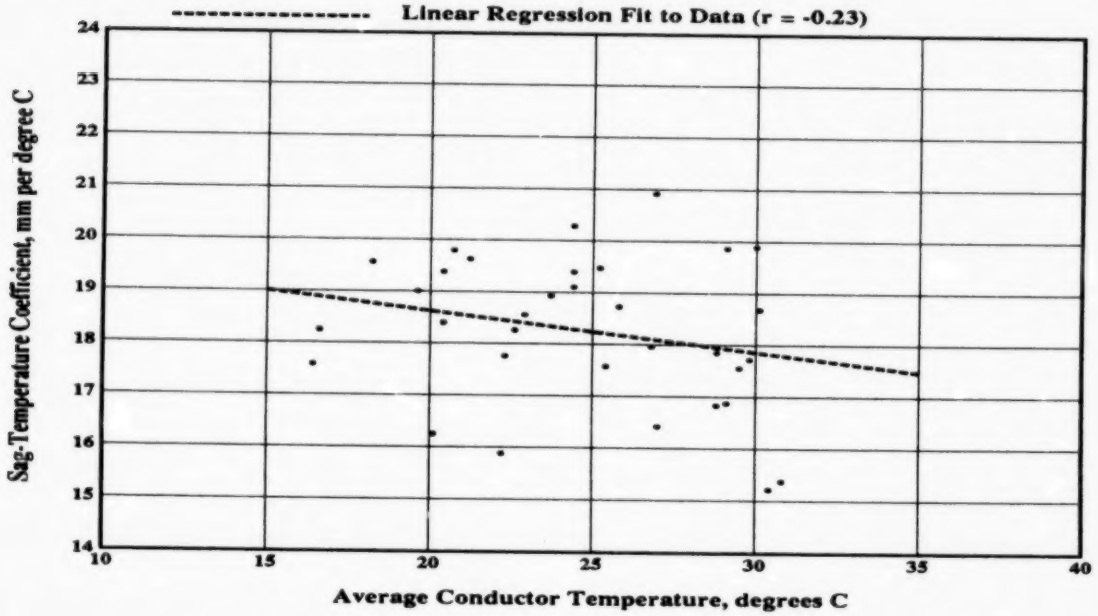

Figure 3: 24-Hour Average Sag-Temperature Coefficient versus Average Conductor Temperature

The scatter about the mean is large. There is, however, a slight slope to the data. A linear regression of sag-temperature coefficient against temperature produces a weak (-0.227) correlation to the regression line plotted. A careful examination of values in Table 3 shows the reason: The change of sag with temperature is not constant, but tends to change with temperature.

Table 3
Change in Sag-Temperature Coefficient With Temperature
Calculation for Essa Test Line Short Span with 39.3 kg Instruments

Temperature	Ruling Span Sag	Δ Sag	Accurate Sag	Δ Sag
20°	4.001 m	---	3.8557 m	---
30°	4.159 m	15.8 mm/°C	4.0455 m	19.0 mm/°C
40°	4.313 m	15.4 mm/°C	4.2338 m	18.8 mm/°C
50°	4.462 m	14.9 mm/°C	4.4199 m	18.6 mm/°C

Thus, the trend to lower observed sag-temperature coefficient with higher temperature is physically correct. The magnitude is in close agreement with the accurate model.

IMPROVED WIND AND THERMAL MODELS

Existing line rating practice applies several factors to OOLM predictions of wind speed. Depending on line height, a sheltering factor of 0.7 to 0.9 is used. A spatial-variability factor of 0.8 is also recommended, along with a constant wind angle of 20° to the conductor. To balance these reduction factors, a minimum wind speed of 4 km/hr is substituted whenever predictions fall below this level.

The conservative factors lead to bias in the predictions of conductor temperature. This bias was identified in previous work and is studied again in the next section. We feel that the bias should be reduced by changes to the wind angle model.

Theoretical support for improved wind angle models has been found in air pollution literature /8/. Figure 4 shows a "Wind-Direction Range Climatology" from a station in Idaho.

The lines of constant standard deviation, or "isopleths", show that the wind-direction standard deviation is between 40° and 50° for most day-time periods in the summer. The effect of this variation in wind direction can be seen from Equation 3, which averages over Nusselt ratios for variable wind direction to obtain an effective Nusselt ratio.

$$\frac{Nu}{Nu_{90}} = \frac{1}{\sqrt{2\pi}\sigma_\theta} \int_{-6\sigma}^{6\sigma} e^{-\theta^2/2\sigma_\theta^2} (0.05+0.95\sin^2\theta)^{0.25}\, d\theta \qquad (3)$$

Figure 5 shows the relationship between wind-direction standard deviation and corresponding wind angle. A 45° standard deviation around a zero-degree wind angle provides as much cooling as a steady 30° wind angle. We studied the influence of wind-angle standard deviation in the OOLM models by changing wind angle to 30° from 9AM to 3PM.

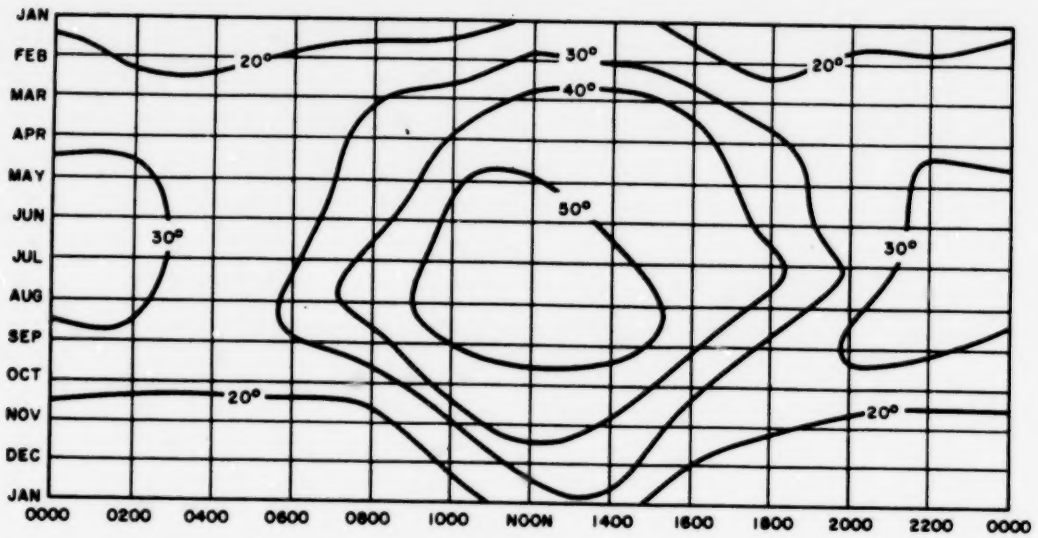

Figure 4: Wind-Direction Range Climatology for National Reactor Testing Station, Idaho. Isopleths show lines of constant 15-minute wind-angle standard deviation.

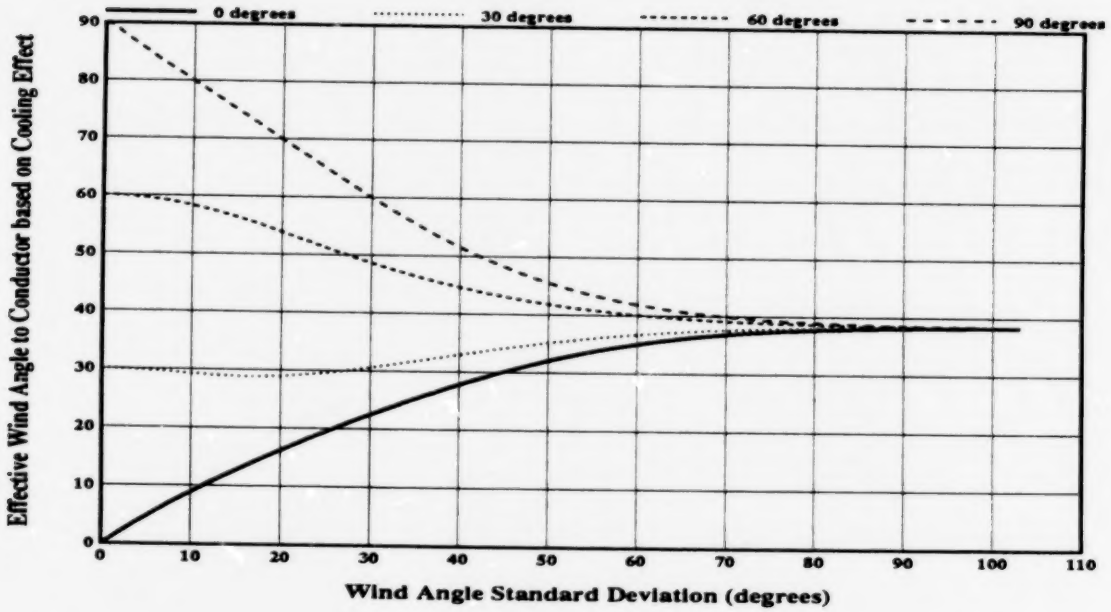

Figure 5: Effective Wind Angle vs Angle Standard Deviation for Four Wind Angles to Conductor.

We expect that the conductor temperature will increase with decreasing wind speed, provided that ambient temperature and solar input remain constant. In Figure 6a, we show the predicted conductor temperature T_c versus the perpendicular component of the wind, V_{90} for a solar input of 814 w/m^2, ambient temperature T_a of 30°C and conductor current of 260 A. Three different models are used. The House and Tuttle method forms the basis of the Transmission Design Method /3/. The AMPAC program /2/ is based on Morgan /6/ with a number of approximations. The Holman /7/ data were obtained from a recent textbook on heat transfer. The Holman model incorporates improved modeling of the empirical relations between flow and heat transfer, including a method for combining effects of natural and forced convection.

Figure 6b shows a similar comparison, using the new (1986) IEEE/ANSI Standard /9/. The standard is based on a modified House and Tuttle approach, with different assumptions for solar input, conductor emissivity and absorptivity. The IEEE method suggests absorptivity and emissivity values of 0.5; the S&T Design and AMPAC approaches use 0.7 and 0.9. The peak solar input to the conductor is over 1000 W/m^2 in the IEEE model for the Barrie area; we assume a maximum value of only 814 W/m^2. The IEEE method gives temperatures that are 2-5 C° higher than the S&T Design method using its recommended inputs.

In Figure 6a, the Morgan /2/ and House and Tuttle /3/ models track each other very closely. The only deviation is seen at very low wind speeds, with the Morgan method predicting a higher temperature under natural convection. The Holman model gives lower temperatures at low winds because it considers the combined cooling effects of forced and natural convection. Both Morgan and House and Tuttle use the larger of the two terms. This can be improved by the following process:

Compute equivalent vertical wind component from natural convection:

$$V_{NC} = 0.0166\sqrt{d\ (Tcond - T_{amb})} \tag{4}$$

Combine the vertical wind, V_{NC}, the vertical wind from the ground V_{vert}, the cross-wind V_{cross} and the axial wind V_{axial} as follows:

$$V_{eff} = \sqrt{(V_{vert} + V_{NC})^2 + V_{cross}^2 + 0.05V_{axial}^2} \tag{5}$$

The 0.05 factor for the longitudinal component models the cooling effect of axial winds with good accuracy /10/. The V_{eff} is used with a 90° wind angle in the S&T or AMPAC models. If the vertical component of natural wind V_{vert} is unknown, it can be set to zero. In that case, results are identical to our existing wind-angle model.

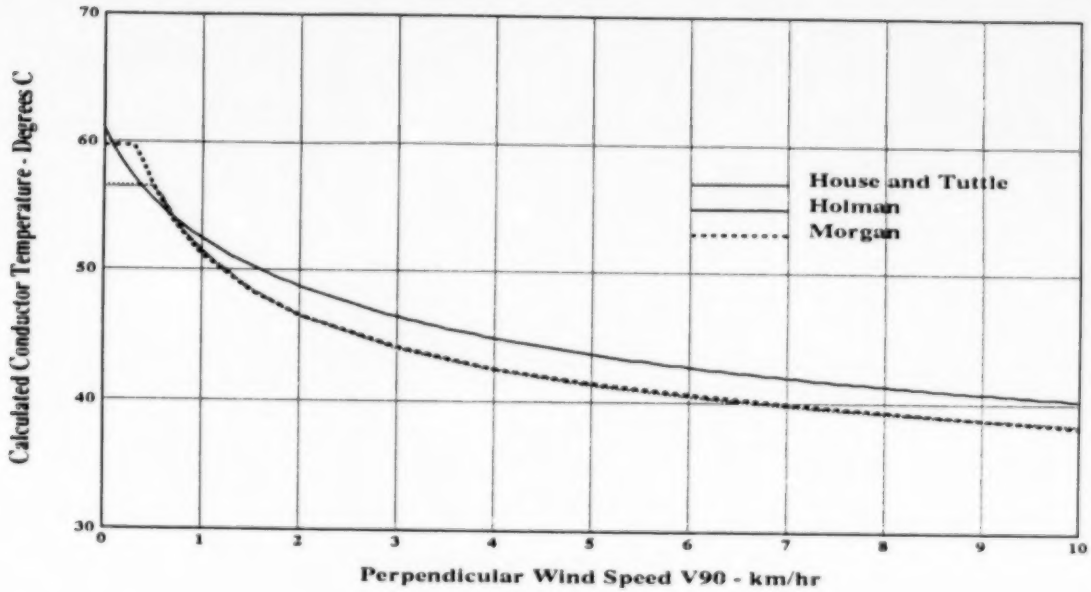

Figure 6a: Predicted Conductor Temperature vs Wind Speed Using Three Cooling Models.

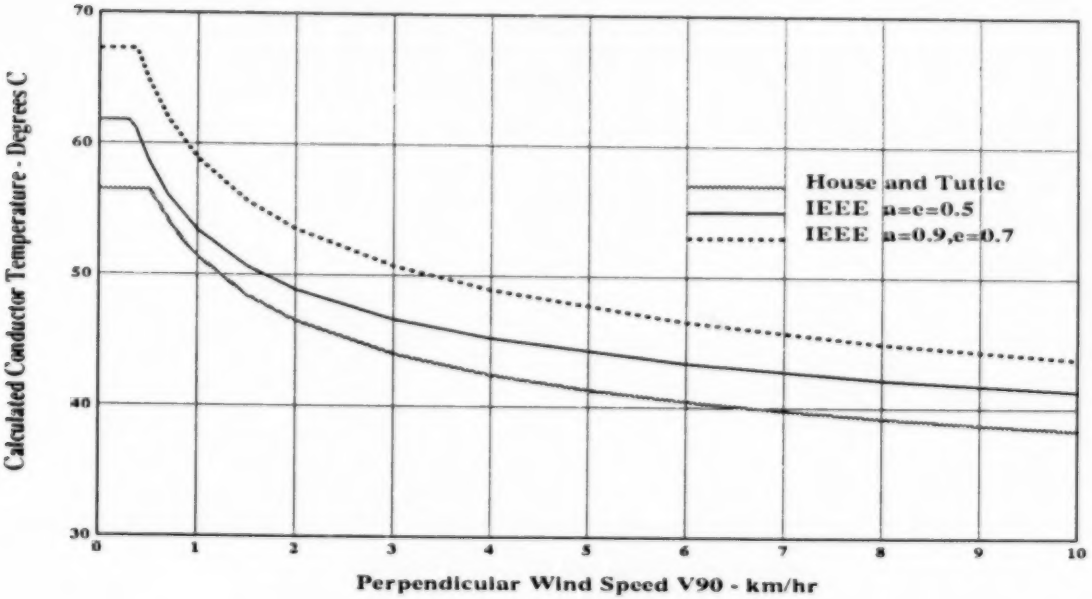

Figure 6b: Predicted Conductor Temperature vs Wind Speed Using Three Cooling Models.

PERFORMANCE OF OOLM AND SITE PREDICTIONS

Figure 7 shows predicted conductor temperatures versus wind speed for three values of ambient temperature - 20°, 25° and 30°C. A constant solar input of 814 W/m^2 was assumed for the calculation. We also sorted all the measured conductor temperature T_c values that were taken during conditions when solar input was high and T_a within 1 C°). The experimental T_c values are plotted against the effective wind velocity V_{eff} from Equation 5, using $V_{NC} = 0$.

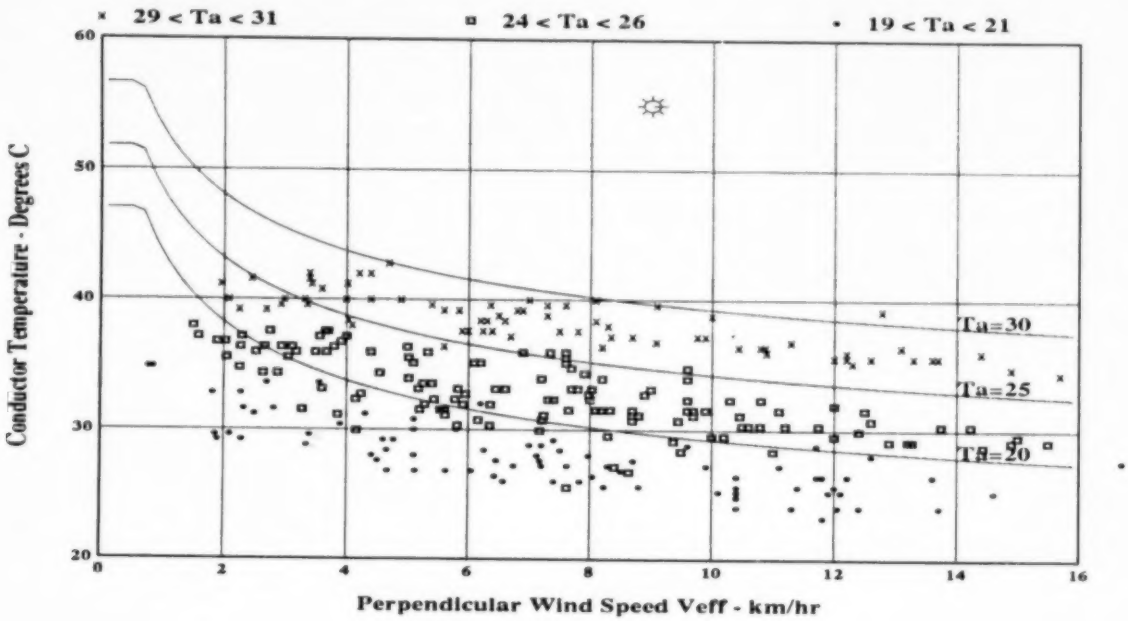

Figure 7: Predicted and Observed Conductor Temperature vs Wind Speed At Two Ambient Temperatures. Solar Input Exceeds 600 W/m^2.

The experimental data values fall below the corresponding theoretical lines. Most of the deviations result from differences between actual and assumed solar input. Some additional differences from theory are seen at the low wind-speed range of 2-3 km/hr, particularly for T_a = 30°C.

When the variability of solar input is eliminated, the agreement between theory and measurement is better. The low-solar results in Figure 8 that the data points are scattered within about 2 C° of the theory, even at low wind speeds.

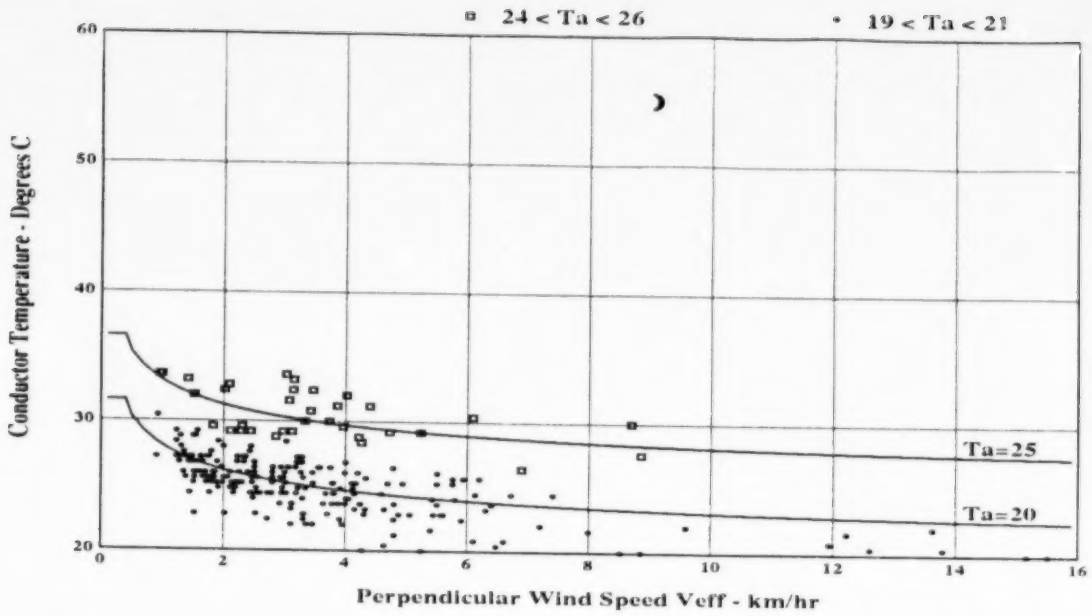

Figure 8: Predicted and Observed Conductor Temperature vs Wind Speed at Two Ambient Temperatures. Solar Input Less Than 100 W/m^2.

Figures 9-11 show histograms of the differences between predicted and observed conductor temperatures for the entire operating season. In Figure 9, we see that 50% of the predictions based on site data are within 0.5 C° of the measured conductor temperature. This provides good confidence in the thermal model that we used, given the correct input data.

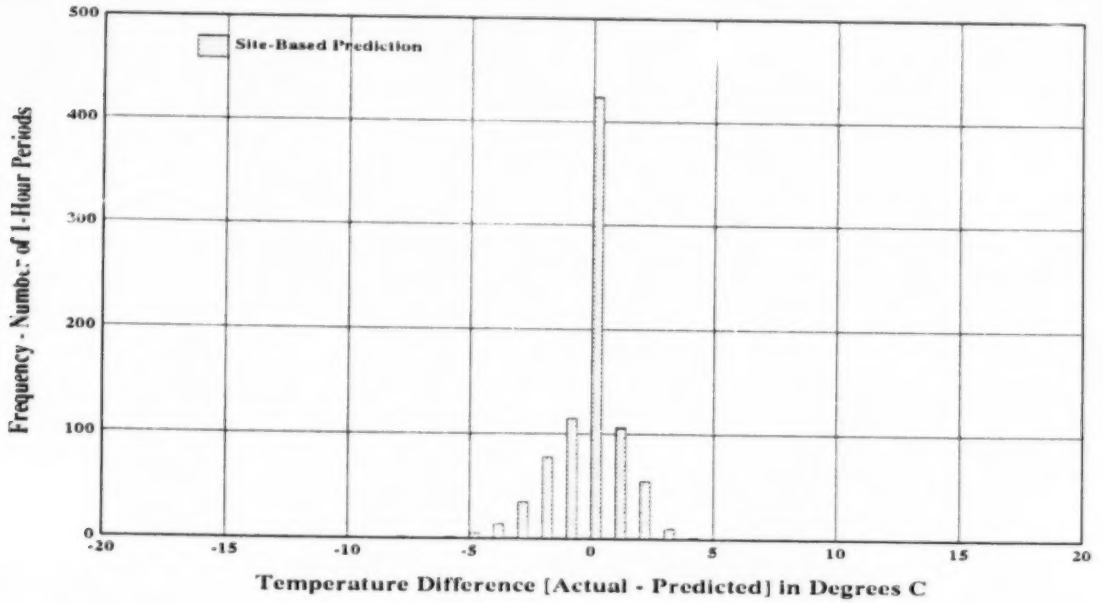

Figure 9: Histogram of Differences between Predicted and Observed Conductor Temperatures. Predictions use Site Data.

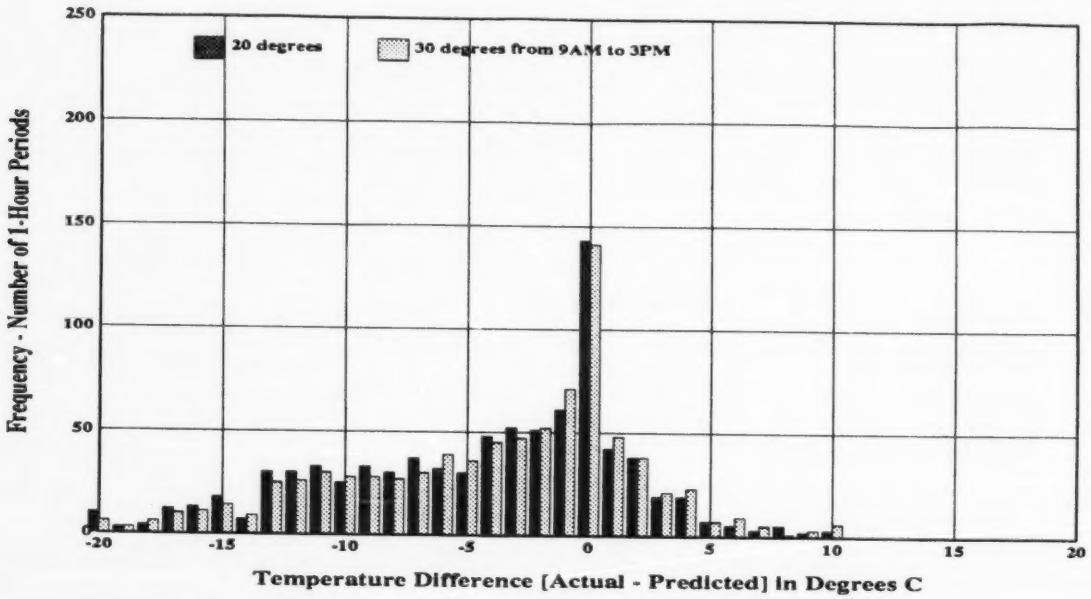

Figure 10: Histogram of Differences between Predicted and Observed Conductor Temperatures. Predictions use 1-Hour OOLM Data.

Figure 10 shows the predictions based on 1-Hour OOLM meteorology forecasts. The distribution is much wider and has a slight conservative bias. A wind angle θ of 20°, a sheltering factor K_h of 1.0 and a spatial variability factor K_s of 0.8 were used to model our unsheltered test line. The distribution shape is improved slightly when a wind angle of 30° is assumed from 9AM to 3PM every day.

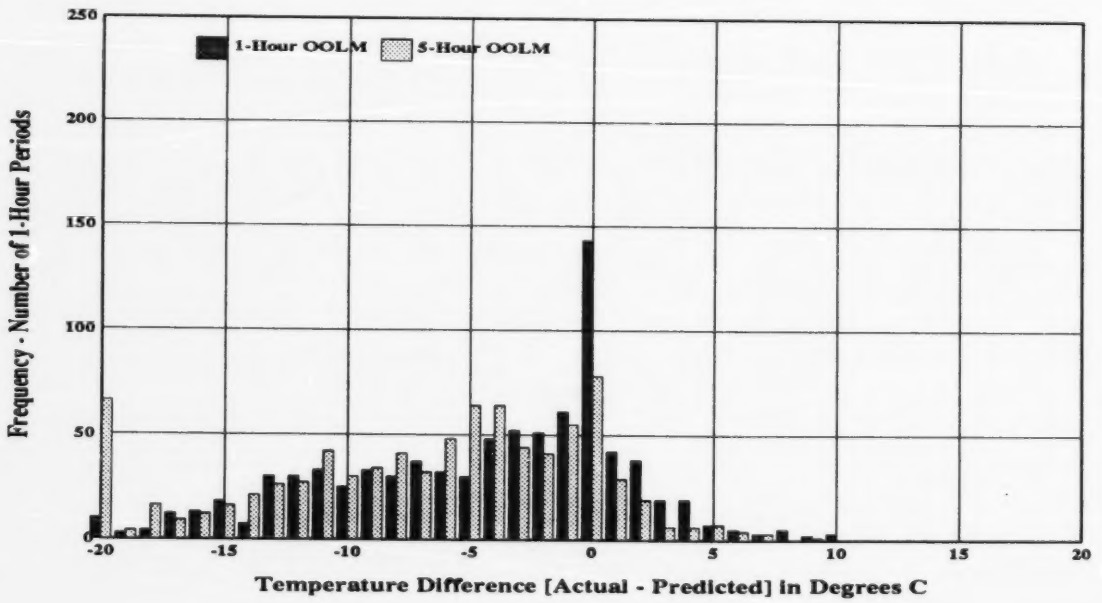

Figure 11: Histogram of Differences between Predicted and Observed Conductor Temperatures. Predictions use 1-Hour and 5-Hour OOLM Data.

Figure 11 shows the differences between 1-Hour and 5-Hour OOLM predictions. As intended, the 5-Hour predictions show conservative bias, with a 66 hourly estimates being more than 20C° higher than the observed conductor temperature. There are still 18 hours, however, in which the predicted temperature was more than 4 C° too low.

Appendix 2 provides a detailed listing of the 37 1-hour periods during which the OOLM 1-hr prediction understated observed conductor temperature by more than 4 C°. In most cases, the ambient temperature prediction was lower than the site measurement by this amount. Two-thirds of the periods occurred at night.

CONCLUSIONS

Sag-temperature coefficient on our test line was measured to be 18.7 ±0.1 mm/°C. This is in good agreement with accurate theory (18.9 mm/°C) and does not agree with ruling-span predictions (15.6 mm/°C). The small changes in clearance have a significant impact on the temperature rating of 115-kV lines. If the Essa Test Line was rated at 49°C using the ruling-span approximation, it should be de-rated to 40°C using the accurate model of Appendix 1.

When site measurements are used to calculate conductor temperature, using the House and Tuttle model, the predictions track the observed conductor temperature very closely. There is very little difference between House and Tuttle /3/ and Morgan /2/ models of conductor ampacity for natural wind speeds.

The effective wind angle to the conductor is probably too low in day-time summer use of OOLM weather data. A value of 30° is supported by air-pollution studies in Idaho. This value leads to slightly better predictions, but considerable bias and scatter still exist.

RECOMMENDATIONS

Discontinue use of the existing sag-tension programs when evaluating clearance of lines with unequal spans. Replace ruling-span approximations with the accurate model of Appendix 1.

Check thermal ratings of 115-kV lines and change them to reflect the accurate sag-temperature relationships. Lines with the highest ratios of longest to shortest span should receive attention first.

Study the wind-direction range climatology of Ontario. This data should be available from air-pollution literature. If the wind-direction standard deviation exceeds 45° during summer days, an effective wind angle of 30° to the conductor can be used.

ACKNOWLEDGEMENTS

Jakov Motlis of Design and Development - Transmission pointed out the inadequacy of a single "sag-temperature coefficient" in clearance calculations and provided insight into design standards for correct, and incorrect, application of the ruling-span approximation.

The Out-Of-Limits Monitoring weather data, and references for wind climatology, were provided by the staff of Power System Operations - Resource Utilization - Meteorology.

The data analysis was performed on a multi-user UNIX system, commissioned and supported by Martin Green. The computer power sped up development of the iteration plan in Appendix 1 and allowed greater scope in the work.

Approved:

A.F. Baljet
Manager
Electrical Research Department

WAC:aba

Prepared:

W.A. Chisholm
Engineer/Physicist
Transmission and Special Projects Section
Electrical Research Department

J.S. Barrett
Physicist
Transmission and Special Projects Section
Electrical Research Department

REFERENCES

1. W.A. Chisholm and J.S. Barrett, "Overhead Conductor Ampacity Studies II: Essa Test Line Results, Summer 1985", Ontario Hydro Research Division Report 86-91-K.

2. M. Cenanovic, "Calculation of Continuous and Emergency Conductor Ampacities", Ontario Hydro Research Division Report 74-192-H

3. Transmission Design Methods Number 9, "Ampacity of ACSR Transmission Lines", November 1972.

4. W.A. Chisholm and J.S. Barrett, "Overhead Conductor Ampacity Studies III: Predicted and Observed Conductor Temperatures, Essa Test Line Results, Summer 1986", Ontario Hydro Research Division Report 86-360-K.

5. P.F. Winkleman, "Sag-Tension Computations and Field Measurements of Bonneville Power Administration", **AIEE Transactions on Power Apparatus and Systems**, February 1960.

6. V.T. Morgan, "Rating of Bare Overhead Conductors for Continuous Currents", **Proc. IEE**, Vol 114, No 10, October 1967, pp 1473-1482.

7. J.P. Holman (New York: McGraw Hill), **Heat Transfer**, 6th Edition, 1986.

8. D.H. Slade (Editor), **Meteorology and Atomic Energy 1968**, U.S. Atomic Energy Commission TID-24190, 1968.

9. IEEE/ANSI Standard 738-1986, "IEEE Standard for Calculation of Bare Overhead Conductor Temperature and Ampacity Under Steady-State Conditions", IEEE, December 1985.

10. V.T. Morgan, "The Overall Convective Heat Transfer from Smooth Circular Cylinders", **Advances in Heat Transfer**, Vol 2, (New York: Academic Press), 1975, p 242.

APPENDIX 1

ACCURATE CALCULATION OF SAGS WITHOUT RULING-SPAN APPROXIMATION

A method for calculating insulator swings in two dimensions to calculate sag-temperature relationships for straight transmission lines.

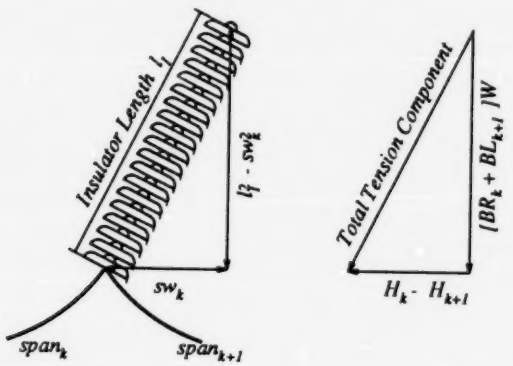

NOMENCLATURE

TWR_k	tower separation in span k
S_k	span length k (horizontal distance between attachment points)
sw_k	horizontal swing of the insulator at the right-hand end of span k (positive for swing left)
H_k	horizontal component of tension in span k
BL_k	distance from left end of span to low point
BR_k	distance from right end of span to low point
Y_k	elevation of right end of span k above the left end
l_I	insulator length
lo_k	length of span k at reference temperature
AE	spring constant (conductor cross section × elastic modulus)
W	conductor weight per unit length
α	coefficient of thermal expansion

At reference temperature T_0, the insulators are assumed to be hanging vertically so that all spans have the same horizontal component of conductor tension H_0. At this reference temperature and tension, the length of conductor in each span k is lo_k. At any other temperature the following relationships hold:

$$l_k = lo_k\left[1 + \frac{H_k - H_0}{AE} + \alpha(T - T_0)\right] \qquad \text{(A1)}$$

This describes the conductor length in span k as related to the change in elastic and thermal strains.

$$l_k = S_k\left[\frac{\sinh(x_k)}{x_k} + \frac{1}{2}\left[\frac{Y_k}{S_k}\right]^2\right] \tag{A2}$$

where $x_k = \left[\frac{WS_k}{2H_k}\right]$. This describes the conductor length in span k as related to the catenary variables.

Combining Equations A1 and A2 and expanding, we obtain an expression for S_k that is sufficiently accurate for calculating the derivatives $\partial S_k/\partial H_k$:

$$S_k = lo_k\left[1 + \frac{H_k - H_0}{AE} + \alpha(T - T_0) - \frac{W^2S_k^2}{24H_k^2} - \frac{1}{2}\left[\frac{Y_k}{S_k}\right]^2\right] \tag{A3}$$

$$\frac{\partial S_k}{\partial H_k} = lo_k\left[\frac{1}{AE} + \frac{W^2S_k^2}{12H_k^3}\right] \tag{A4}$$

Referring to Fig A1, the tension balances at each suspension insulator between spans k and $k+1$ are given by:

$$H_k - H_{k+1} = (BR_k + BL_{k+1})W\frac{sw_k}{\sqrt{l_l^2 - sw_k^2}} \tag{A5}$$

where

$$BR_k = \frac{S_k}{2} + \frac{H_k}{W}\frac{Y_k}{S_k} \tag{A6}$$

$$BL_{k+1} = \frac{S_{k+1}}{2} - \frac{H_{k+1}}{W}\frac{Y_{k+1}}{S_{k+1}} \tag{A7}$$

For n spans there are $n-1$ tension-balance equations having the form of Equation A5. The other constraint necessary to solve for the tensions in every span is that the sum of all the spans is equal to the sum of all the tower separations. There are thus n equations in n unknowns.

On each iteration, a new set of tensions H is obtained and is used to generate accurate span lengths using hyperbolic formulae. The iteration procedure itself consists of using the tensions H from the previous iteration as a starting point, and expanding Equation A5 to first order in all of the H values. The result is:

$$\delta H_k - \delta H_{k+1} = (BR_k + BL_{k+1})W\left[\frac{1}{\sqrt{l_l^2 - sw_k^2}} - \frac{sw_k^2}{(\sqrt{l_l^2 - sw_k^2})^3}\right]\left[\sum_{l=1}^{k}\frac{\partial S_l}{\partial H_l}\right]\delta H_l \tag{A8}$$

The BR and BL terms do not require expansion since they change very little and converge rapidly if recalculated on each iteration.

The last factor in Equation A8 is from the following relationship:

$$\delta(sw_k) = \sum_l \frac{\partial sw_k}{\partial H_l} \delta H_l = \sum_{l=1}^{k} \frac{\partial S_l}{\partial H_l} \delta H_l \qquad \text{(A9)}$$

These derivatives are given by Equation A4.

The constraint that the sum of the span lengths must equal the line length between dead-end structures leads to the following equation:

$$\sum_{l=1}^{n} \frac{\partial sw_k}{\partial H_l} \delta H_l = 0 \qquad \text{(A10)}$$

The $n-1$ equations having the form of Equation A8, together with Equation A10 constitute n linear equations in the n unknowns δH. This set of equations is solved on each iteration until convergence is achieved. A deceleration factor is required on the first few iterations when there are many spans in the section of transmission line. Program SWING is based on this algorithm and has been used on sections over 40 spans long without convergence problems.

BIRDCAGING

Some modifications to the above method are required for conductors operating above the birdcaging temperature. The birdcaging temperature T_B and tension H_B will vary slightly from span to span because higher conductor tension will result in higher birdcaging temperature and birdcaging tension. However, this effect is small and we may use the values of T_B and H_B for the ruling span as calculated by a program capable of evaluating them for a given conductor loading history and limiting compressive stress in the aluminum strands [A1].

Making the approximation that all of the spans birdcage at the same temperature T_B and tension H_B as the ruling span, Equation A1 becomes:

$$l_k = lo_k \left[1 + \frac{H_B - H_0}{AE} + \alpha(T_B - T_0) + \frac{H - H_B}{A_s E_s} + \alpha_s (T - T_B) \right] \qquad \text{(A11)}$$

where $A_s E_s$ is the spring constant of the ACSR's steel core and α_s is the steel core's thermal expansion coefficient. A similar change is required in Equation A3 and the AE in Equation A4 becomes $A_s E_s$.

REFERENCE

[A1] J.S. Barrett, S. Dutta and O. Nigol, **A New Computer Model of ACSR Conductors**, IEEE Trans., Vol. PAS-102, No. 3, March 1983, pp. 614-621.

APPENDIX 2 - Listing of 1-Hour Periods During Which OOLM-Based Prediction Understated Conductor Temperature by more than 4 degrees C.

Day Of Year	Tc	Tcalc site	T1hr 20deg	T1hr 30deg	T5hr	V90 site	Vwind OOLM	Sol site	Sol OOLM	Ta site	Ta Cur OOLM	
190.0000	32.0	32.3	26.6	26.6	26.6	5.4	4.2	0.0	0.0	26.9	18.0	294.0
193.2500	23.6	26.8	16.8	16.8	21.9	1.4	6.0	355.2	0.0	10.7	9.0	304.0
196.6667	30.4	32.5	20.5	20.5	28.0	26.6	4.0	771.6	814.0	26.7	0.0	262.0
199.2083	31.6	34.7	25.5	25.5	28.5	2.9	4.0	588.2	0.0	21.2	18.0	272.0
199.2500	34.4	37.9	24.7	24.7	28.7	3.3	7.4	691.4	0.0	24.1	19.0	268.0
199.4167	39.2	39.2	31.5	30.0	37.4	4.4	13.3	676.1	814.0	27.1	19.0	266.0
199.4583	37.6	39.9	33.5	32.0	38.5	7.5	13.3	771.6	814.0	29.5	21.0	268.0
202.7083	41.2	45.7	36.0	36.0	36.5	2.5	16.1	695.2	814.0	30.9	25.0	252.0
202.8333	34.4	34.2	25.1	25.1	25.1	4.3	14.8	145.1	0.0	27.8	21.0	264.0
202.8750	32.8	33.6	24.0	24.0	24.0	2.0	9.4	49.7	0.0	26.3	19.0	264.0
202.9167	29.2	30.0	22.9	22.9	22.9	3.9	9.9	0.0	0.0	25.0	18.0	266.0
202.9583	29.6	29.9	24.6	24.6	24.6	2.9	4.7	0.0	0.0	24.3	18.0	264.0
203.0000	28.4	29.4	23.1	23.1	23.1	2.9	5.9	0.0	0.0	23.7	17.0	266.0
203.0417	28.0	28.6	22.5	22.5	22.5	3.2	7.4	0.0	0.0	23.2	17.0	264.0
203.0833	27.2	27.8	22.0	22.0	26.6	3.9	6.0	0.0	0.0	22.8	16.0	266.0
203.1250	28.0	27.9	20.9	20.9	22.1	3.5	6.6	0.0	0.0	22.6	15.0	268.0
203.1667	29.2	28.7	19.6	19.6	23.0	2.6	7.2	0.0	0.0	22.7	14.0	266.0
203.2083	29.2	29.4	20.1	20.1	23.1	1.6	4.2	0.0	0.0	22.2	13.0	268.0
203.2500	28.4	27.7	17.8	17.8	22.9	3.1	6.7	0.0	0.0	22.1	12.0	268.0
204.0417	24.4	23.6	18.3	18.3	23.5	1.5	4.0	0.0	0.0	16.1	11.0	270.0
204.0833	22.0	23.6	17.4	17.4	24.7	2.5	4.0	0.0	0.0	17.4	10.0	272.0
210.8333	36.8	35.0	25.4	25.4	26.0	3.8	14.8	320.9	0.0	25.9	21.0	274.0
211.4167	39.6	40.4	32.2	30.6	35.3	4.3	12.1	798.3	814.0	26.7	19.0	272.0
211.4583	37.6	37.5	33.1	31.5	37.1	4.9	10.2	565.3	814.0	26.9	19.0	270.0
211.5000	38.4	38.4	30.3	29.0	34.3	5.6	17.2	576.8	814.0	28.3	19.0	272.0
211.6667	35.2	36.7	31.1	31.1	32.1	7.4	14.7	573.0	814.0	27.7	19.0	272.0
211.8333	29.6	30.4	23.5	23.5	23.7	5.1	13.1	194.8	0.0	23.8	19.0	270.0
211.8750	28.0	27.1	22.8	22.8	23.1	5.6	11.0	30.6	0.0	22.4	18.0	270.0
211.9167	27.2	25.9	23.2	23.2	23.9	4.0	9.4	0.0	0.0	20.8	18.0	270.0
215.2500	24.8	25.3	19.8	19.8	23.8	2.3	6.0	3.8	0.0	18.3	13.0	282.0
215.8333	29.6	32.4	25.6	25.6	25.6	1.3	6.4	156.6	0.0	20.9	19.0	280.0
216.8333	28.4	28.0	23.4	23.4	23.4	2.4	6.9	80.2	0.0	20.0	17.0	282.0
224.3333	32.4	35.3	28.2	28.2	31.7	2.5	10.8	466.0	814.0	22.2	14.0	282.0
224.4167	33.2	37.4	27.9	26.4	30.9	4.5	13.3	695.2	814.0	24.7	15.0	280.0
224.4583	36.8	39.2	28.7	27.2	31.7	4.9	13.7	737.2	814.0	26.7	16.0	278.0
224.5000	36.0	36.5	28.0	26.5	31.0	5.7	15.5	523.3	814.0	26.8	16.0	276.0
224.5417	33.2	34.9	28.7	27.2	30.8	8.0	16.7	530.9	814.0	26.5	17.0	278.0

DISTRIBUTION

R.W. Whitehead	Transmission Operations	U4E1
E.M. Kurak	Transmission Operations	U5E1
D.E. Amm	Transmission Operations	U5E6
A.J. Carreira	Transmission Operations	U7C1
H.W. Parish	Transmission Operations	U2A1
I.R. Menzies	Transmission Operations	E2C1
J.J. Clifton	Transmission Operations	E2A3
K.D. Noble	Transmission Operations	U7C5
R.A. Brown	Design and Development - Transmission	H9A1
B.A. Oliver	Design and Development - Transmission	H9C1
J.F. Wilson	Design and Development - Transmission	H9F27
J.R. Meale	Design and Development - Transmission	H9F27
M.S. Nashid	Design and Development - Transmission	H9D27
D.J. Horrocks	Design and Development - Transmission	H9G27
J. Motlis	Design and Development - Transmission	H9G25
L.J. Rubino	System Planning	H4G27
E.G. Neudorf	System Planning	H4D27
J.A.R.Service	System Planning	H4A22
J.P. Bayne	System Planning	H4F21
J.S. McConnach	System Planning	H4A25
T. Rusnov	System Planning	H4G1
R. Wilson	Health and Safety	H2A27
F.A. Perttula	Georgian Bay Region	
R. Cochrane	Public Relations	H19A5
P.C. Maenhaut	Power System Operations	A6A6
J.A. Findlay	Power System Operations	A6H8
A.J. Harris	Power System Operations	A6H1
D.R. Cowbourne	Power System Operations	A6A8
P.M. Murphy	Power System Operations	A6A7
A.E. Boyer	Power System Operations	A6E1
R.W. Miller	Power System Operations	A6E2
A. Fraser	Power System Operations	A6E2
O.T. Melo	Chemical Research	KD138
D.G. Havard	Mechanical Research	KB223
A.F. Baljet	Electrical Research	KR120
O. Nigol	Electrical Research	KR139
C.C. Erven	Electrical Research	KR271
M. Cenanovic	Electrical Research	KL206
K.H. Von Bank	Electrical Research	KR262
P. Redden	Electrical Research	KR262
D.E. Parsons	Electrical Research	KR262
J.S. Barrett (5)	Electrical Research	KR139
W.A. Chisholm (5)	Electrical Research	KR260

Public Reference Centre
Editorial Section (2)
Office Copies (2)
Extra Copies (5)